HHS Public Access

Author manuscript

J Control Release. Author manuscript; available in PMC 2018 February 10.

Published in final edited form as:

J Control Release. 2017 February 10; 247: 153–166. doi:10.1016/j.jconrel.2016.12.038.

An Intraocular Drug Delivery System Using Targeted Nanocarriers Attenuates Retinal Ganglion Cell Degeneration

Lei Zhao[#1], **Guojun Chen**[#2], **Jun Li**[1,3,4], **Yingmei Fu**[1,5], **Timur A. Mavlyutov**[1], **Annie Yao**[1], **Robert W. Nickells**[7,8], **Shaoqin Gong**[2,6,8,*], and **Lian-Wang Guo**[1,8,*]

[1]Department of Surgery, 5151 Wisconsin Institute for Medical Research, University of Wisconsin-Madison, 1111 Highland Ave, Madison, WI 53705, U.S.A.

[2]Department of Materials Science and Engineering, and Wisconsin Institutes for Discovery, University of Wisconsin-Madison, Madison, WI 53715, U.S.A.

[3]Department of Ophthalmology, The First Hospital of China Medical University, Shenyang, 110001, China.

[4]Department of Ophthalmology, The 3rd People's Hospital of Dalian, Dalian, 116033, China

[5]Shanghai Key Laboratory of Psychotic Disorders, Shanghai Mental Health Center, Shanghai Jiao Tong University School of Medicine, 600 Wanping Nan Road, Shanghai, 200030, China.

[6]Department of Biomedical Engineering, University of Wisconsin-Madison, Madison, WI 53715, U.S.A.

[7]Department of Ophthalmology and Vision Sciences, University of Wisconsin-Madison, 1300 University Ave, Madison, WI 53706, U.S.A.

[8]McPherson Eye Research Institute, University of Wisconsin-Madison, Madison, WI 53705, U.S.A.

[#] These authors contributed equally to this work.

Abstract

Glaucoma is a common blinding disease characterized by loss of retinal ganglion cells (RGCs). To date, there is no clinically available treatment directly targeting RGCs. We aim to develop an RGC-targeted intraocular drug delivery system using unimolecular micelle nanoparticles (unimNPs) to prevent RGC loss. The unimNPs were formed by single/individual multi-arm star amphiphilic block copolymer poly(amidoamine)–polyvalerolactone–poly(ethylene glycol) (PAMAM–PVL–PEG). While the hydrophobic PAMAM–PVL core can encapsulate hydrophobic drugs, the hydrophilic PEG shell provides excellent water dispersity. We conjugated unimNPs with

[*]Corresponding authors: Lian-Wang Guo, Ph.D., Department of Surgery, University of Wisconsin, 1111 Highland Avenue, WIMR 5151, Madison, WI 53705, Tel: +1 608 262 6269, Fax: +1 608 262 3330, guo@surgery.wisc.edu, Shaoqin Gong, Ph.D., Department of Biomedical Engineering and Wisconsin Institutes for Discovery, University of Wisconsin–Madison, 330 North Orchard St, Madison, WI, 53715, Tel: +1 608 316 4311, shaoqingong@wisc.edu.

Competing Interests: The authors have declared that no competing interests exist.

the cholera toxin B domain (CTB) for RGC-targeting and with Cy5.5 for unimNP-tracing. To exploit RGC-protective sigma-1 receptor (S1R), we loaded unimNPs with an endogenous S1R agonist dehydroepiandrosterone (DHEA) as an FDA-approved model drug. These unimNPs produced a steady DHEA release *in vitro* for over two months at pH 7.4. We then co-injected (mice, intraocular) unimNPs with the glutamate analog N-methyl-D-aspartate (NMDA), which is excito-toxic and induces RGC death. The CTB-conjugated unimNPs (*i.e.*, targeted NPs) accumulated at the RGC layer and effectively preserved RGCs at least for 14 days, whereas the unimNPs without CTB (*i.e.,* non-targeted NPs) showed neither accumulation at nor protection of NMDA-treated RGCs. Consistent with S1R functions, targeted NPs relative to non-targeted NPs showed markedly better inhibitory effects on apoptosis and oxidative/inflammatory stresses in the RGC layer. Hence, the DHEA-loaded, CTB-conjugated unimNPs represent an RGC/S1R dual-targeted nanoplatform that generates an efficacious template for further development of a sustainable intraocular drug delivery system to protect RGCs, which may be applicable to treatments directed at glaucomatous pathology.

Graphical abstract

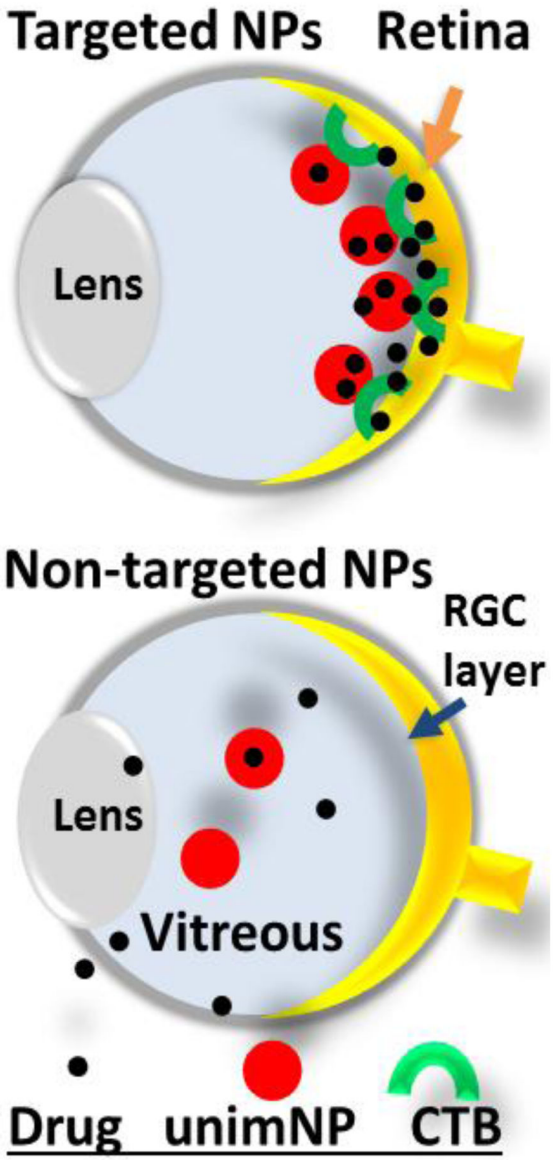

Schematic: Intraocular drug delivery system using nanoparticles targeting retinal ganglion cells (RGCs).

CTB: non-toxic cholera toxin B domain.

unimNP: unimolecular micelle nanoparticle

Keywords

Targeted drug delivery; unimolecular micelles; retina; ganglion cell targeting; excitotoxicity; sigma-1 receptor; cholera toxin B domain

1. INTRODUCTION

Glaucoma is the most common cause for irreversible blindness worldwide. While high intraocular pressure is considered the major risk factor for causing optic nerve damage, it is the death of retinal ganglion cells (RGCs) that manifests visual field deficits[1]. Current treatments for glaucoma focus on reducing the intraocular pressure. However, these methods can provide temporary relief and are not always effective at attenuating neurodegeneration. There is no clinical modality to treat glaucoma by directly targeting RGCs to protect them from degeneration.

Ample *in vitro*[2-6] and *in vivo*[7-10] evidence indicates that the sigma-1 receptor (S1R) is a potential intervention target for the prevention of RGC death. S1R was discovered to be a ligand-operated chaperone, and when activated, is generally pro-survival[11]. A long-held mystery in its binding with diverse natural and synthetic ligands was rationalized by the newly reported crystal structure of this protein [12]. The S1R agonist (+)-pentazocine reduced RGC loss in a mouse model of diabetic retinopathy[8] and in primary cultures of RGCs exposed to excitotoxins[3], while S1R knockout mice exhibit greater RGC loss versus wild type control in a model of acute optic nerve damage[7]. Most recently, an anti-inflammatory function of S1R activation was also found in retinal macroglial and microglial cells[13-15]. Taken together, these studies suggest that S1R protects RGCs' viability by alleviating oxidative stress, excitotoxicity, ER stress, and/or inflammation.

Despite numerous reports demonstrating a neuro-protective role of S1R, there have been a lack of investigations with a focus specifically on therapeutic methods exploiting the neuro-protective potential of S1R in the retina. Some high-affinity S1R ligands (*e.g.,* pentazocine, PRE084, and SKF10047) are often used for mechanistic studies, but they are not approved for human use. Dehydroepiandrosterone (DHEA), a neurosteroid, is an endogenous compound identified as a S1R agonist[16, 17]. Importantly, it is also an FDA-approved drug. A recent report indicates that DHEA protects retinal neurons by alleviating excitotoxicity[18], consistent with earlier studies showing that DHEA, via S1R, protects the retina from damage in a ischemia/reperfusion model[17, 19]. Thus DHEA is a promising therapeutic for retinal protection.

As every drug has off-target effects at certain concentrations, systemic delivery is often associated with complications caused by side effects. Intraocular injection is a standard clinical practice. But this invasive treatment is accompanied with risks such as bleeding, pain, infection, and retinal detachment[20]. An intraocular delivery method enabling prolonged drug release would reduce the required frequency of injections and hence the associated risks.

Nanoparticles (NPs) are an effective platform for drug delivery[21]. Nanomedicine has exhibited a great deal of versatility and is being used to treat a variety of disease conditions, especially cancer. Several groups have used NPs for intraocular drug delivery and shown protective effects for the retina [22-24]. However, a key obstacle remains unsolved. As drug/NPs are diluted in the vitreous and quickly cleared out of the eye, drug efficacy and durability can be adversely compromised. To overcome this problem, in the current study,

we conjugated NPs with the RGC-targeting cholera toxin B domain (CTB) so that NPs could be sequestered and accumulated at the RGC layer. CTB binds to GM1 ganglioside, which is highly enriched on the RGC surface, and then undergoes internalization. As such, fluorescent CTB has been recently established as an RGC tracer which shows little (if any) labeling of non-neuronal tissues[25-28]. We engineered a unique NP—*i.e.,* unimolecular micelle NP (unimNP) as shown in Figure 1A—that offers excellent *in vivo* stability, versatile bioconjugation, and prolonged drug release[29-36]. Using DHEA as a model drug loaded in CTB-conjugated unimNPs (*i.e.,* targeted NPs) and an RGC excitotoxicity model, we tested the efficacy of an RGC-targeted intraocular drug delivery strategy. We found that targeted NPs are more efficacious than non-targeted NPs in preventing RGC loss. This intraocular drug delivery nanoplatform reconciles the benefits of targeted NPs and the neuroprotective function of S1R.

2. MATERIALS and METHODS

2.1 Materials

Poly(amidoamine) (PAMAM, ethylenediamine core; G4) dendrimer, valerolactone (VL), tris(2–carboxyethyl)–phosphine (TCEP), stannous (II) octoate ($Sn(Oct)_2$), and FITC-cholera toxin B (CTB) were purchased from Sigma–Aldrich (St. Louis, MO, USA). Cy5.5 dye was obtained from Lumiprobe Corporation (Hallandale Beach, FL, USA). The heterobifunctional poly(ethylene glycol) (PEG) derivatives, methoxy–PEG–COOH (mPEG–COOH, M_n = 5 kDa), maleimide–PEG–COOH (Mal–PEG–COOH, M_n = 5 kDa), and COOH–PEG–NH_2 (M_n = 5 kDa), were purchased from JenKem Technology (Allen, TX, USA). 2–Iminothiolane (Traut's reagent), 4–Dimethylamino pyridine (DMAP) and 1,3–dicyclohexylcarbodiimide (DCC) were purchased from Thermo Fisher Scientific (Rockford, IL, USA) and used without further purification. Other reagents were purchased from Thermo Fisher Scientific (Fitchburg, WI, USA).

2.2 Synthesis of PAMAM–PVL–OH

PAMAM–OH (10 mg, 0.7 μmol), VL (138 mg, 1.4 mmol), and $Sn(Oct)_2$ (0.57 μg, 1.4 μmol) were added into a two–neck flask. The reaction was carried out at 120 °C for 24 h under argon. The resulting mixture was dissolved in THF and the solution was added dropwise into methanol to yield pale yellow precipitates. The final product PAMAMA–PVL–OH was dried under vacuum.

2.3 Synthesis of Cy5.5–PEG–COOH

Cy5.5–NHS (5 mg, 7 μmol) and NH_2–PEG–COOH (29 mg, 5.8 μmol) were dissolved in 5 mL DMF. Triethylamine (TEA) was used, as reported previously[4-6], to adjust the pH of the solution to 8-8.5. The reaction was carried out at room temperature under dark for 24 h. The resulting reaction solution was added dropwise into cold ethyl ether and the precipitates were recrystallized in hot 2–propanol. The final product was dried under vacuum.

2.4 Synthesis of PAMAM–PVL–PEG–OCH_3/Cy5.5/Mal

PAMAM–PVL–PEG–OCH_3/Cy5.5/Mal was synthesized by reacting PAMAM–PVL–OH with mPEG–COOH, Cy5.5–PEG–COOH, and Mal–PEG–COOH in 10 mL of DMF in the

presence of DCC and DMAP. The molar ratio of reactants (PAMAM–PVL–OH:mPEG–COOH:Cy5.5–PEG–COOH:Mal–PEG–COOH:DCC:DMAP) was set at 1:48:3:12:70:7. The reaction was carried out at room temperature for 48 h and the by–product, dicyclohexylcarbodiurea, was removed by filtration. The resulting solution was added dropwise into 10 fold of cold diethyl and the impurities were removed by dialysis against DI for 48 h using cellulose tubing (molecular weight cut-off, 15 kDa). The resulting polymer PAMAM–PVL–PEG–OCH_3/Cy5.5/Mal was freeze–dried.

2.5 Preparation of DHEA-loaded unimNPs (non-targeted NPs)

The DHEA-loaded unimNPs were prepared using a dialysis method. Briefly, PAMAM–PVL–PEG–OCH_3/Cy5.5/Mal (20 mg) and DHEA (5 mg) were dissolved in 3 mL of DMSO. Thereafter, 9 mL of DI water were added dropwise into the solution under constant stirring. The resulting solution was stirred for 4 h and the organic solvent and unloaded drug were then removed by dialysis against DI water using cellulose tubing (molecular weight cut-off, 15 kDa) for 48 h. The final DHEA-loaded unimNPs were dried under lyophilization.

2.6 Synthesis of CTB-conjugated and DHEA-loaded unimNPs (DHEA-loaded CTB-unimNPs, i.e., targeted NPs))

Cholera toxin B (CTB) was first reacted with Traut's agent to generate the functional thiol group for further conjugation. Briefly, CTB and Traut's agent (molar ratio: 1:10) were mixed in PBS for 4 h at 4 °C. DHEA-loaded unimNPs were then added into this solution and the resulting reaction mixture was stirred for another 16 h. Thereafter, the impurities were removed by dialysis against DI water for 24 h using cellulose tubing (molecular weight cut-off, 100 kDa). The final product was obtained after lyophilization.

2.7 Characterization

^{1}H NMR spectra of all polymer products were recorded on a Varian Mercury Plus 300 spectrometer in $CDCl_3$ or DMSO–d_6. Fourier transform infrared (FT–IR) spectra were recorded on a Bruker Tensor 27 FT–IR spectrometer. Molecular weights (M_n and M_w) and polydispersity indices (PDI) of the polymers were determined by gel permeation chromatography (GPC) equipped with a refractive index detector, a viscometer detector, and a light scattering detector (Viscotek, USA). DMF with LiBr (0.1 mmol/L) was used as a mobile phase with a flow rate at 1 mL/min. The morphologies of the unimNPs were determined by dynamic light scattering (DLS, ZetaSizer Nano ZS90, Malvern Instrument, USA) and transmission electron microscopy (TEM, FEI Tecnai G^2 F30 TWIN 300 KV, E.A. Fischione Instruments, Inc. USA). The DHEA loading level, defined as the weight percentage of DHEA in the DHEA-loaded unimNPs, was measured by high-performance liquid chromatography (HPLC) using ultraviolet (UV) detection at 210 nm at 40 °C[37]. Water and acetonitrile (v/v=7/3) at a constant flow rate of 1 mL/min was used as a mobile phase.

2.8 Determination of in vitro drug release profiles

The *in vitro* DHEA release profiles from DHEA-loaded unimNPs, either without CTB (non-targeted NPs) or with CTB (targeted NPs), were determined at pH 7.4 in PBS buffer as well

as at pH 5.3 in an acetate buffer solution (ABS). Release was performed and quantified following our published method[38]. Briefly, DHEA-loaded unimNPs in the medium buffer (1 mg/mL, 5 mL) were enclosed in a cellulose membrane dialysis bag (molecular weight cut–off, 15 kDa). The dialysis bag was immersed in 50 mL of the release medium, which was then kept in a horizontal laboratory shaker (100 rpm) at a constant temperature of 37°C. At predetermined time intervals, samples of 3 mL were collected and replaced with fresh media of the same volume. Amounts of DHEA in the collected samples were measured by HPLC as described above in Section 2.7.

2.9 Animals

All animal procedures conformed to the NIH Guide for the Care and Use of Laboratory Animals and were in compliance with the ARVO Statement for the Use of Animals in Ophthalmic and Vision Research. Animal protocols were approved by the Institutional Animal Care and Use Committee at the University of Wisconsin–Madison (protocol# M02102). All surgeries were performed under isoflurane anesthesia (through inhaling, flow rate 2 ml/min). Animals were euthanized in a chamber gradually filled with CO_2. C57BL/6 mice were purchased from the Jackson Laboratory (Bar Harbor, ME). Animals were maintained on a 4% fat diet (8604 M/R, Harkland Teklad, Madison, WI) and subjected to standard light cycles (12 h/12 h light/dark). Both male and female mice in the age range of postnatal days 30–60 were used in experiments.

2.10 Intravitreal injection of NMDA and test agents

Intravitreal injection of NMDA is a widely used model of induced RGC death[39]. Animals were classified into four groups (at least 6 mice in each). In group 1, vehicle control (DMSO in PBS) was injected with a Hamilton syringe into one eye, and NMDA (from a DMSO stock) dissolved in PBS was injected into the contralateral eye of the same mouse. In group 2, a mixture of NMDA and non-targeted NPs was injected into the left or right eye (randomly assigned) of a mouse. In group 3, a mixture of NMDA and targeted NPs was injected into the the left or right eye. In group 4, a mixture of NMDA and empty NPs (CTB-unimNPs without DHEA) was injected into the left or right eye. Injection was performed as previously described[40]. The total volume of each injection was 2 μL, containing 0.5 μg DHEA and 2 μg unimNP, and/or 40 mM NMDA. These intravitreal injection experiments were repeated at least three times.

2.11 Preparation of retinal cryosections and whole mounts

Cryosections were prepared according to our published method[41]. At various time points after injection, animals were euthanized by CO_2 asphyxiation followed by cervical dislocation. Eyeballs were marked in the superior portion with a cautery, enucleated immediately and dissected to remove the anterior segment. Eyecups were fixed in 4% paraformaldehyde for 7 h, and then cryoprotected in 30% sucrose in PBS for another 14 h, all at 4 °C. Cryosections of 10 μm each were cut through the optic nerve in the superior-inferior plane of the eyecups frozen in the optimum cutting temperature (O.C.T.) embedding medium (Sakura Finetek 4583, Sakura Finetek USA, Inc., Torrance, CA), and used for 4′,6-diamidino-2-phenylindole (DAPI) (Thermo Fisher Scientific) staining, immunostaining, or

terminal deoxynucleotidyl transferase dUTP nick end labeling (TUNEL), as described in the following sections.

Whole mounts were prepared as previously described[40]. Eyeballs of euthanized mice were marked in the superior portion, enucleated, and fixed in 4% paraformaldehyde for 1h. After rinsing in PBS, eyecups were generated, and retinas were dissected out and placed with the ganglion cell layer (GCL) facing up onto a Superfrost Plus slide (Thermo Fisher Scientific). Four additional relaxing cuts were made to allow the retina to lay flat. The whole mounts were used for BRN3A and DAPI staining and then thoroughly rinsed in PBS before being covered with Immu-mount (Thermo Fisher Scientific), coverslipped and stored at 4°C in the dark.

2.12 Nuclei counting in the RGC layer on vertical sections and on whole mounts

Cell counting on vertical sections—A cell in the RGC layer with a round or oval nucleus with minimal appearance of condensed heterochromatin and at least one prominent nucleolus was considered a neuron[39]. The number of neurons was evaluated by counting DAPI-stained nuclei following our published method with minor modifications[42]. Briefly, on each sagittally oriented section, the regions of 0–1000 μm and 1000–2000 μm from the optic nerve head were designated as central and mid-peripheral, respectively. Neuronal nuclei were manually counted in each (500 μm length of retina) of the four fields chosen in the central and mid-peripheral regions of the RGC layer flanking the optic nerve head. The counts from all 3-4 sections of the same animal were averaged, and the means from 6–9 animals were then averaged to calculate the mean and SEM for each group of animals.

Cell counting on whole mounts—Counting was performed based on our previous publication[43] with minor modifications. Images were captured on the four wholemount sections generated by 4 relaxing cuts, and nuclear counts were obtained from 12 distinct fields (0.09 mm^2)(see Figure S1) for each retina and averaged together. Only rounded nuclei with at least one nucleolus, typical of both RGCs and amacrine cells in this layer, were included in the counts. Endothelial cells exhibiting elongated nuclei and no nucleolus, and densely staining astrocytes were excluded.

2.13 Immunohistochemistry and fluorescence microscopy

Immunostaining was performed on cryosections following our previously described method[41] with minor modifications. Briefly, retinal sections were permeabilized with 1% Triton X-100 in PBS for 20 min, blocked with 10% normal goat serum (Cat#71–00–27; Kirkegaard & Perry Laboratories, Gaithersburg, MD) for 2 h at room temperature, and then incubated with a primary antibody overnight at 4°C. Sources and dilutions of primary antibodies were as follows: Mouse anti-BRN3A (Millipore, Cat.#MAB1585), 1:50; rabbit anti-IBA1 (Waco, 019-19741), 1:400; mouse anti-GFAP (Millipore, MAB3402), 1:100; and rabbit anti-pPERK (Thr981) (Santa Cruz, sc-32577), 1:100. After rinsing the section 3×, a secondary antibody (Alexa-488 conjugated goat-anti-rabbit or Alexa-594-conjugated goat-anti-mouse) at 2 μg/ml was applied at room temperature for 2 h. Sections were then rinsed 3×, counterstained with DAPI for 5 min, and then mounted in Prolong Gold mounting medium (Invitrogen, Carlsbad, CA) and cover-slipped. The slides were left in the dark

overnight and then sealed using clear nail polish (Electron Microscopy Sciences, Hatfield, PA). Images were then taken with a Nikon Eclipse Ti microscope with a DS-Qi1 camera using ×10 or ×40 objective lenses and analyzed by Nikon Elements software. For quantification of immunofluorescence intensities, areas of GFAP, IBA-1, and pPERK immunopositivity were derived by thresholding images (Image J) captured under uniform imaging conditions and expressed as a fraction of the area of the chosen field (500 μm retinal length) across the INL/GCL region. Images of immunostaining without a primary antibody were used as background control of thresholding.

Wholemount immunostaining for BRN3A was performed as previously described[44], with minor modifications. Briefly, fixed eyecups were incubated in PBS containing 0.5% Triton-X100 and 2% donkey serum (Jackson ImmunoResearch, Inc.) for 1.5 h at room temperature. They were then transferred into the same buffer containing primary antibody overnight at 4°C. The eyecups were thoroughly rinsed in PBS with 0.5% Triton-X100, and then fixed for an additional 10 minutes in 4% paraformaldehyde. Eyecups were rinsed in PBS and whole mounted onto Fisher Plus slides, and then incubated in 0.5% Triton-X100 and 2% donkey serum with 1:500 secondary antibody (Jackson ImmunoResearch) for 2 h at room temperature. The whole mounts were rinsed in PBS and stained with 300 ng/ml DAPI for 5 minutes at room temperature. After a final wash with PBS, the slides were coverslipped with Immu-Mount and used for fluorescence microscopy.

2.14 TUNEL assay

Assays were performed using an *in situ* cell death detection kit (Roche, Indianapolis, IN, USA) following our published method[45]. Frozen retinal sections were stained with the kit to assess DNA fragmentation as an indicator for dying cells. For quantification, 3–4 sections from each animal were used, and on each section, three fields (each of 500 μm retinal length) in the central, middle, and peripheral regions were imaged for counting of TUNEL-positive cells. This was a binary decision. Cells were either positive or negative. The counts from all sections of the same animal were averaged, and the means from 6–9 animals were then averaged to generate the mean and S.E. for the group of animals.

2.15 Quantitative real-time PCR (qRT-PCR)

Retinas were isolated at various time points after injection and RNA was extracted using Trizol (Qiagen, Valencia, CA), as described previously[46]. Purified mRNA (1 μg) was used for the first-strand cDNA synthesis using an iScript cDNA synthesis kit (Bio-Rad) and quantitative RT-PCR was performed using the 7500 Fast Real-Time PCR System (Applied Biosystems, Carlsbad, CA). Each cDNA template was amplified in triplicate using SYBR Green PCR Master Mix (Applied Biosystems, Carlsbad, CA). Transcript quantification was based on standard curves of each target amplimer to determine absolute transcript quantities, and normalized to GAPDH. Cycling conditions were 95°C (15 seconds) and 60°C (60 seconds) for 40 cycles with a dissociation step. Primer sequences are presented in Table S1. All primers crossed at least one intron/exon boundary[42, 47], and all amplimers were sequenced to confirm identity.

2.16 Statistical analysis

The required sample sizes in animal experiments were calculated based on estimates of mean differences, variances, and power. Data of cell counting, immunohistochemistry, TUNEL assay, and RT-PCR were analyzed using ANOVA (OriginLab, Northampton, MA). Significance was set at $P < 0.05$. In all graphical representations, the error bars indicate standard error of the mean (SEM).

3. RESULTS

3.1 Synthesis and characterization of multi-arm star amphiphilic block copolymer PAMAM–PVL–PEG–Cy5.5/CTB

A schematic of the final targeted NP is shown in Figure 1A. Figure 1B shows the synthetic scheme of the multi-arm star amphiphilic block copolymer PAMAM–PVL–PEG–Cy5.5/CTB. First, PAMAM–PVL–OH was prepared by ring-opening polymerization of the VL monomer using PAMAM–OH (4th generation) dendrimer as the macroinitiator. The ^{1}H NMR spectrum shown in Figure 1C confirmed the chemical structure of the PAMAM–PVL–OH polymer. The peaks at (a) 1.65 ppm, (b) 2.36 ppm, and (c) 4.12 ppm were attributed to the protons in the PVL main chains. The signal at (c') 3.65 ppm corresponding to the terminal methine protons of PVL could also be identified. The peaks ranging from 2.55 to 3.45 ppm were ascribed to the PAMAM core of PAMAM–PVL–OH. The FT-IR spectrum analysis (Figure S2 in the supporting information) also confirmed the successful synthesis of PAMAM–PVL–OH. The peaks at 1542 cm^{-1} and 1648 cm^{-1} were assigned to N–H bending and C=O stretching of the amide bonds of PAMAM, respectively. The peak located at 1720 cm^{-1} was ascribed to the ester bonds of the PVL arms. According to the ^{1}H NMR spectrum, the average number of repeat units of the PVL arms was calculated to be 26 based on the intensity ratio of the peaks at (c) 4.12 ppm and (c') 3.65 ppm. Based on Eq. 1, the average number of arms (# arm) per PAMAM–PVL–OH was determined to be 33 by comparing the molecular weights of PAMAM–OH and PMAMA–PVL as measured by gel permeation chromatography (GPC) (Table 1).

$$\#\mathrm{arm} = \left(Mn_{\mathrm{PAMAM-PVL-OH}} - Mn_{\mathrm{PAMAM-OH}}\right)/Mn_{\mathrm{PVL}} \quad \text{Eq. 1}$$

In the next step, three types of hydrophilic PEG—namely mPEG–COOH, Mal–PEG–COOH, and Cy5.5–PEG–COOH (synthesized via amidization of Cy5.5–NHS and NH_2–PEG–COOH, ^{1}H NMR spectrum shown in Figure 1D)—were conjugated to PAMAM–PVL–OH via an esterification reaction forming the multi-arm star amphiphilic block copolymer PAMAM–PVL–PEG–OCH_3/Cy5.5/Mal. The Mal functional groups were used for further conjugation of the CTB targeting ligand, while the methoxyl groups present in PEG–OCH_3 were used to control the molar ratio of the Mal groups and Cy5.5 dye molecules at the surface of the unimNPs, which subsequently controlled the numbers of CTB and Cy5.5 dye per unimNP. Theoretically, two Cy5.5 dye molecules were conjugated onto each PAMAM–PVL–PEG–OCH_3/Cy5.5/Mal polymer. ^{1}H NMR spectra clearly demonstrated the formation of PAMAM–PVL–PEG–OCH_3/Cy5.5/Mal (Figure 1E). In addition to the peaks of PVL, a peak at 3.65 ppm was observed due to the protons of the oxyethylene units of PEG.

The signal located at 7.06 ppm was ascribed to the Mal groups. The characteristic peaks of Cy5.5 dye were observed around 7.5–8.5 ppm. GPC results further confirmed the successful synthesis of multi-arm star amphiphilic block copolymer PAMAM–PVL–PEG–OCH_3/Cy5.5/Mal. As shown in Table 1, the molecular weight of PAMAM–PVL–PEG–OCH_3/Cy5.5/CTB was measured to be 252,317 Da, which was significantly larger than that of PAMAM–PVL–OH (99,450 Da), thus indicating the successful formation of PAMAM–PVL–PEG–OCH_3/Cy5.5/Mal. Similarly, the average number of arms per PAMAM–PVL–PEG–OCH_3/Cy5.5/Mal was calculated to be 32 based on the molecular weights measured by GPC. This result is in a good agreement with the previous reports on the number of arms in PAMAM-based dendritic amphiphilic block copolymers[33] (Eq. 2).

$$\#\mathrm{arm} = \left(Mn_{\mathrm{PAMAM-PVL-PEG-OCH_3}/Cy5.5/\mathrm{Mal}} - Mn_{\mathrm{PAMAM-PVL-OH}}\right)/Mn_{\mathrm{PEG}} \quad \text{Eq. 2}$$

Since CTB is sensitive to organic solvents, and the drug loading process requires the use of organic solvents, DHEA was encapsulated into the unimNPs before CTB conjugation. The DHEA-loaded unimNPs were prepared using a standard dialysis method[48] and the DHEA loading level (defined as the weight percentage of DHEA in DHEA-loaded unimNPs) was 18.6%. In order to conjugate the targeting ligand CTB onto the unimNPs, the active amine groups ($-NH_2$) on the surface of CTB were first converted into thiols in the presence of Traut's agent. Afterwards, the thiolated CTB was conjugated onto the DHEA-loaded unimNPs via a thiol–Mal click reaction. The molar ratio of DHEA-loaded unimNPs and CTB was set at 1:2 (2 CTB molecules per unimNP).

3.2 Micellar properties of unimNPs and in vitro *DHEA drug release from DHEA-loaded unimNPs*

The multi-arm star amphiphilic block copolymer PAMAM–PVL–PEG can form stable unimNPs in an aqueous solution. As shown in Figure 1F, the average hydrodynamic diameter of the unimNPs measured by DLS was 62 nm (PDI = 0.14). The TEM images of unimNPs presented in Figure 1G showed a clear core–shell structure with an average diameter of around 34 nm. The different sizes measured by TEM and DLS were due to the fact that DLS measured the hydrodynamic diameter of the unimNPs, while TEM measured the diameter of the dehydrated ones.

NPs are typically taken up by cells through an endocytosis process involving endosomes and lysosomes. While the pH values of extracellular matrix and cytosols are neutral, pH values inside endosomes and lysosomes range from 4.5 to 6.5. We thus determined the DHEA release profiles from DHEA-loaded unimNPs at pH 7.4 as well as pH 5.3, a commonly used condition to mimic the acidic microenvironment of the endocytic compartments [34, 49, 50]. As shown in Figure 1H, sustained drug release was observed at both pH conditions. Specifically, less than 50% of DHEA was released from the unimNPs after 2 weeks at pH 7.4, while nearly 86% was released at pH 5.3. DHEA was released faster at an acidic condition, most likely due to the faster degradation of the hydrophobic PVL core via acid-catalyzed hydrolysis. Significantly, DHEA was released steadily up to 2 months at pH 7.4 (Figure S3). The observed sustainable drug release is desirable, allowing for prolonged

protective effect on RGCs. Another favorable feature of the targeted NPs is that the CTB conjugation on unimNPs does not interfere with DHEA release, as evidenced by almost identical DHEA release profiles from non-targeted and targeted NPs at the same pH (Figure 1H).

3.3 Targeted NPs but not non-targeted NPs are accumulated at the RGC layer after intravitreal injection

After the micellar properties and drug release profiles of the DHEA-loaded unimNPs were fully characterized, their RGC-targeting effect was tested *in vivo*. Both targeted NPs (i.e., DHEA-loaded and CTB-conjugated unimNPs) and non-targeted NPs (i.e., unimNPs loaded with DHEA but lacking CTB) were tested. Both targeted and non-targeted NPs were conjugated with Cy5.5 dye, which was used to localize these NPs. To test the RGC protective effect of the unimNPs, we performed intravitreal injection of N-methyl-D-aspartate (NMDA), a model widely used to study RGC degeneration and protection[39]. NMDA is a non-hydrolyzable analog of glutamate, which binds NMDA receptors and elicits excitotoxicity and RGC death. NMDA and non-targeted NPs (control) were co-injected into the left or right eye (randomly assigned) of one group of mice, while equivalent amounts of NMDA and targeted NPs were injected into a separate group of age-match mice. At 1, 3, and 7 days post injection, mice were euthanized and retinal sections or whole mounts were prepared for fluorescence microscopy. As shown in Figure 2A, at 1 day post injection, intense signals from targeted NPs (Cy5.5, red) were observed at the RGC layer, which co-localized with CTB (FITC, green). However, in control eyes injected with non-targeted NPs, the Cy5.5 signal was barely detectable. At 7 days post injection, Cy5.5 fluorescence from targeted NPs remained strong at the RGC layer, whereas it was not detected in control eyes injected with non-targeted NPs. Further microscopic analysis (Figure 2B) showed that while the Cy5.5 label of the targeted NPs (white) over-imposed with the fluorescence of the CTB targeting ligand (green), it was also in juxtaposition with BRN3A-labeled nuclei. This data confirms the penetration of targeted NPs into the RGC layer, as BRN3A is a transcription factor localized in the nucleus that is specifically expressed in RGCs[27]. An overview (Figure 2C) of Cy5.5 distribution in the entire eye indicated accumulation of targeted NPs specifically at the RGC layer but at no other tissues in the eye. No accumulation of non-targeted NPs was observed (Figure S4). To confirm the results from vertical sections, we also performed whole mount fluorescence imaging. Targeted NPs were consistently found retained on the RGC side of the whole mounts, whereas much less Cy5.5 fluorescence from non-targeted NPs were detected (Figure 3A). Moreover, the juxtaposition of targeted NPs to BRN3A-labeled RGCs suggested efficient RGC targeting by these NPs (Figure 3B).

3.4 Targeted NPs but not non-targeted NPs are able to effectively and durably protect RGCs from NMDA-induced cell death in the retina

To compare the therapeutic efficacy between targeted NPs and non-targeted NPs, experiments were performed as described above. Eyeballs were collected at 1, 3, 7, and 14 days post injection, either fixed for preparation of retinal whole mounts and cryosections, or processed without fixation for retinal tissue homogenates (for quantitative RT-PCR). The numbers of nuclei counted on retinal whole mounts are presented in Figure 3C and re-plotted as fold changes in Figure 3D for convenience of comparison. At 7 days post

injection, while NMDA alone reduced RGCs (BRN3A-positive) to ~10% of vehicle (DMSO) control, DHEA delivered with targeted NPs preserved the cell number at ~45% (Figure 3D). In stark contrast, DHEA in non-targeted NPs did not significantly prevent RGC loss. Similarly, at 14 days, targeted NPs still maintained the cell number at >40%, while non-targeted NPs did not protect cells from NMDA-induced death. Furthermore, we confirmed that the protective effect was produced by DHEA, as indicated by the comparison between targeted NPs (i.e., CTB-unimNPs loaded with DHEA) and empty NPs (i.e., CTB-unimNPs with no DHEA loaded) (Figure 3, E and F). Namely, CTB-unimNPs *per se* did not show an effect on the RGC number, which was ~400 per mm^2 in mice either injected with NMDA only (no NPs, Figure 3C) or co-injected with empty NPs (Figure 3F) at day 7 or day 14.

In parallel, we also used a different method, nuclei counting on vertical sections, to estimate RGC loss and the protective effect of targeted NPs (Figure 4A). The data are replotted in Figure 4B as fold changes. At 7 days post injection, while NMDA alone reduced the cell number in the RGC layer to 53% of the vehicle (DMSO) control, DHEA in targeted NPs preserved the cell number at ~90%. In contrast, DHEA in non-targeted NPs did not have a statistically significant effect. At 14 days, whereas targeted NPs still maintained a cell number at >80%; non-targeted NPs did not show a protective effect. As only ~50% of the RGC layer cells are RGCs[42], a nearly 50% decrease in total cell number suggests that RGCs were nearly eliminated at 14 days due to NMDA-induced cell death, consistent with the counting result of BRN3A-positive cells (RGCs) on retinal whole mounts (Figure 3D).

To further confirm the preservation of RGCs by targeted NPs, we used quantitative RT-PCR to determine expression levels of RGC-selective genes including *Thy1*, *Nrn1*, and *Nefl*[46]. The data (Figure 4C) show that while NMDA alone (versus vehicle control) reduced mRNA levels of the three genes, targeted NPs significantly prevented this reduction. In contrast, non-targeted NPs did not have a significant effect. The remaining mRNAs of these genes in NMDA-treated retinas were probably contributed by some non-RGC cells, *e.g.,* Müller glia have also been reported to express *Thy1*, especially in injured retinas[51].

We also performed TUNEL assay on retinal sections which measures DNA fragmentation associated with cell death[1]. As indicated in Figure 5, compared to vehicle control, intravitreal injection of NMDA increased TUNEL-positive cells by ~20 fold. Meanwhile, targeted NPs significantly reduced TUNEL-positive cells by more than 50%, whereas the effect of non-targeted NPs was not statistically significant.

Taken together, the foregoing results indicate that targeted NPs, as an intraocular DHEA delivery nanoplatform, outperformed non-targeted NPs in protecting RGCs from NMDA-induced cell death.

3.5 Targeted NPs are more effective than non-targeted NPs in attenuating microglia/macroglia activation and oxidative stress in the retina

Retinal microglia and macroglia (including Müller cells and astrocytes) are commonly implicated as important contributors to RGC death[52]. Interestingly, recent reports demonstrate that S1R plays an inhibitory role in the inflammatory activation of both retinal

microglia and Müller glia[13, 15, 53]. We therefore assessed activation of microglia and macroglia via determination of expression levels of their respective markers, *Iba1*(*Aif1*) and *Gfap*. Indeed, NMDA treatment stimulated the upregulation of both protein and mRNA levels of *Iba1* and *Gfap* (Figure 6). Remarkably, whereas targeted NPs effectively prevented up-regulation of these two markers, the effect of non-targeted NPs was minor and not statistically significant.

It is well documented that NMDA-induced excitotoxicity elevates oxidative stress, which triggers RGC apoptosis[8]. A typical signaling response to oxidative stress is the elevated expression of anti-oxidative genes such as *Nqo1* and *Ho1,* which are therefore often used to monitor increased oxidative stress. One of the most often reported functions of S1R (or S1R agonists) is as an anti-oxidant[54]. We thus determined the expression of *Nqo1* and *Ho1* by qRT-PCR using retinal tissues (Figure 7). The data indicate that while NMDA alone increased mRNA levels of these two genes by 2–3 fold at 3 and 7 days post injection, targeted NPs significantly prevented their up-regulation, while the effect of non-targeted NPs was much less prominent (Figure 7A).

As an ER stress response pathway that is inexorably linked to oxidative stress, PERK activation has been intensively studied in stress response processes. While our data show an increase of pPERK in the retina 3 days after NMDA injection, neither targeted NPs nor non-targeted NPs produced an appreciable effect in attenuating NMDA-induced PERK activation (Figure 7B).

Taken together, these results demonstrated that intravitreally administered DHEA, with targeted NPs as a carrier, was effective in reducing oxidative stress but not PERK pathway activation.

4. DISCUSSION

Glaucoma is a major cause of blindness that will affect 80 million people worldwide by the end of this decade[1]. A hallmark of this disease is RGC degeneration that leads to vision deficit or loss[1]. While surgical treatments exist, there is no preventive clinical care directly targeting RGCs. Thus there is an imperative need for an RGC-protective drug delivery platform that can be conveniently delivered via intraocular injection with low dosing frequency. Rapid advances in nanomedicine have brought about a real possibility for achieving this goal. We have developed a unique type of NP (unimNP) with optimal properties for a drug carrier. Moreover, DHEA, an FDA-approved drug and an endogenous S1R agonist[16], has shown neuro-protective benefits in the brain and retina[17, 18]. To combine these drug/nanocarrier advantages, we conjugated unimNPs with CTB to target RGCs, and loaded DHEA as a model drug to activate S1R. We have thus created a novel RGC/S1R dually targeted nanoplatform. These targeted NPs (*i.e.,* DHEA-loaded and CTB-conjugated unimNPs) formed a retinal drug reservoir at the RGC layer, and produced efficacious and durable protection for RGCs compared to non-targeted NPs in response to NMDA excitotoxicity. As discussed below, this study embodies several innovations.

Polymer micelles are among the most widely studied nanoplatforms due to their unique core–shell structures. The limitation of conventional micelles for *in vivo* applications is their poor stability. Conventional micelles are formed by self-assembly of multiple linear amphiphilic block copolymers. Premature dissociation of the self–assembled multi-molecule polymer micelles can undermine their tissue-targeting capability and cause a burst release of drug, potentially leading to systemic toxicity. However, the unimNP employed in this study can overcome this limitation. All of the components of the unimNP are covalently linked, thus each unimNP is formed by one single molecule, conferring outstanding stability[29, 32]. Moreover, as shown in Figure S3, the unimNPs produced a steady sustained drug release for at least two months, although the release could be accelerated at lower pH (Figure 1H). This is an important trait considering that glaucoma in humans is a chronic condition and hence sustained release is critical for long-term drug efficacy. Furthermore, unimNPs are capable of versatile chemical conjugation with a variety of molecules, including targeting ligands and fluorescent labels, thus enabling their multifunctionality. Taking advantage of these desirable attributes, we conjugated unimNPs with CTB for RGC-targeted drug delivery and Cy5.5 dye for NP-tracing. Therefore, we have generated a novel unimNP drug delivery nanoplatform uniquely tailored for RGC targeting and protection.

Various NPs other than unimNPs have been applied to deliver DNA, siRNA, peptide, or small molecules into the retina[21, 55, 56]. However, these studies were not designed in a targeted manner[57, 58]. Anatomically, the RGC layer is next to the vitreous body, thus it is readily accessible for intravitreally delivered agents. Surprisingly, an RGC-targeting intraocular NP delivery platform has not been reported[58, 59], likely due to the limitations of traditional NPs. On the other hand, targeted delivery can afford multiple benefits including the following: (1) high local drug concentrations producing better drug efficacy, (2) a low risk of side effects because of locally confined drug actions, and (3) low amounts of drug and low dosing frequency needed. In our study, targeted NPs exhibited robust protection for RGC survival whereas non-targeted NPs failed to produce a significant effect. We chose CTB for RGC targeting because it is a recently established RGC tracer[27]. This B domain of cholera toxin lacks the catalytic activity that causes toxicity. Because of its binding activity for GM1 ganglioside that is highly abundant on ganglion neurons, CTB efficiently binds to RGC somata and axons and undergoes lipid raft-mediated internalization[27, 60]. Importantly, our data indicate that while CTB enables sequestration of NPs at the RGC layer, CTB alone did not show toxicity (reduction of cell numbers) (Figure S5). Therefore, CTB facilitates effective RGC targeting of intravitreally delivered CTB-conjugated unimNPs (CTB-unimNPs), and may thus inspire broader applications beyond its common use as an RGC tracer.

Of great interest, an inadvertent benefit of the CTB-unimNPs is the effective accumulation of NPs at the RGC layer which may collectively constitute a retinal drug reservoir. Without CTB, non-targeted NPs are dispersed/diluted in the vitreous body through diffusion after intravitreal injection, with a large portion eventually cleared out of the eye thereby compromising its therapeutic efficacy and imposing a major challenge for intraocular drug administration[20]. Indeed, our data show a minimal RGC-protective effect of non-targeted NPs or free DHEA delivered without NPs (Figure S6). To circumvent this problem, drug-releasing polymer sheets or rods anchored in the vitreous have been tried[20]. However, due

to their bulkiness, these devices often interfere with the normal visual optical path, and when degraded, may produce large amounts of inflammatory degradation products. In contrast, with a hydrophilic outer shell, unimNPs are highly soluble and optically clear in aqueous solutions, thus minimizing interference with vision. Moreover, degradation products of unimNPs with a minute mass are less likely to elicit an inflammatory response In addition, due to their nanoscale sizes (~62 nm in diameter), unimNPs are apparently able to penetrate the inner limiting membrane to function at the RGC layer. The juxtaposition of Cy5.5-labeled unimNPs with RGC nuclei visualized via immunostaining of a specific RGC marker (BRN3A) [27] indicates the presence of NPs either on the surface of or inside RGCs, or in their vicinity. In either case, DHEA released from NPs can produce a functional effect locally on RGCs. A possible scenario is that a portion of the DHEA molecules released from unimNPs may diffuse into other cell layers. This is not expected to impart an adverse effect since DHEA appears to protect retinal cells in general, as evidenced by previous studies without NPs[17-19]. As shown on the whole mount, CTB is distributed not only in the nerve fiber layer (RGC axons, Figure 3A), but also around BRN3A-stained RGC nuclei (Figure S7), consistent with the previous report that CTB is found in the RGC cytosol[27]. It is worth noting, however, CTB is not always associated with Cy5.5 (Figure 3A). While the Cy5.5-labeled puncta are indicative of NPs, dispersed individual NPs (hence less intense fluorescence) may not be detectable. For this reason, some NPs associated with CTB but not forming puncta are not readily discernable. Alternatively, NPs become invisible after losing the Cy5.5 fluorescence; for instance, the ester bond linking these two constituents is broken by esterases, or fluorescence is bleached over time. Nonetheless, our data show profound RGC layer accumulation and, importantly, also RGC-preserving efficacy of targeted NPs carrying DHEA, in contrast to non-targeted NPs with DHEA as well as targeted NPs not loaded with drug. Thus, our study suggests that RGC-targeting via CTB-conjugated unimNPs generates a retinal drug reservoir that enables efficacious and durable RGC protection.

Another innovation in this study is the strategy of RGC/S1R dual targeting. Despite a large body of literature advocating S1R as a potential therapeutic target, there are no reports translating its neuroprotective potential into an applicable method for treating retinal diseases, presumably because of the lack of a viable drug delivery system. The S1R protein is most abundant in the RGCs of mouse, rat, pig, monkey, and human retinas[41]. A neuroprotective role of S1R has been demonstrated in animal models of major neurodegenerative diseases including Alzheimer's disease[61], Parkinson's disease[62], and amyotrophic lateral sclerosis[63, 64]. Particularly important to the current study, a number of *in vitro* and *in vivo* studies[3, 8, 9], including our own[7], demonstrate a protective role of S1R for RGCs under stress. Moreover, some drugs targeting S1R (*e.g.,* fluvoxamine and haloperidol) have proven safe and entered clinical applications for treating psychiatric disorders. Taking advantage of unimNP engineering, we initiated the first translational campaign aiming to develop an intraocular delivery method with S1R as an RGC-protective molecular target. We found that this nanoplatform directed to both a cellular target (RGCs) and a molecular target (S1R) facilitates efficacious precision therapy against RGC neuro-degeneration.

While previous studies using gross retinal samples revealed a S1R-mediated retina-protective effect of DHEA in an ischemia/reperfusion model[17, 19], a S1R-associated effect of DHEA specifically in RGC protection has not been reported. S1R has been identified as a ligand-operated chaperone that has a wide spectrum of molecular functions including modulations of a variety of channels, GPCRs, lipid metabolism, antioxidation, Ca^{2+} homeostasis, and ER stress response[54]. Most recently, S1R was found to suppress retinal microglial and Müller glial reactivity[13, 15], which has been recently recognized as an important etiology of retinal neurodegeneration[52]. Consistently, our data indicated that DHEA-releasing CTB-unimNPs effectively reduced retinal levels of IBA-1, a commonly used marker of activated macrophages and microglia, and levels of GFAP, a marker for activated macroglia including retinal Müller cells and astrocytes. As apoptotic RGCs can cause activation of retinal macroglia and microglia[44], the observed reduction of microglial and Müller glial markers due to the treatment with targeted NPs could be either a direct effect of DHEA, or alternatively, a secondary effect of reduced RGC death. It is known that both activated microglia and macroglia stimulate production of intracellular reactive oxygen species (ROS) and hence oxidative stress, which often triggers antioxidant gene expression. Interestingly, our data showed that while NMDA stimulated the expression of antioxidant genes including *Nqo1* and *Ho1*, targeted NPs effectively reduced the expression of these two genes. The role of S1R in suppressing oxidative stress has been demonstrated in multiple tissues and cells, including retinal microglia and Müller cells[8, 13, 15]. We therefore infer that efficient delivery of DHEA by targeted NPs may have reduced oxidative stress and, in turn, prevented *Nqo1* and *Ho1* up-regulation, at least in part via S1R activation. This outcome may have resulted directly from the S1R anti-oxidative function, or indirectly from inhibition of macroglial and microglial reactivity.

In contrast to the profound inhibitory effect of targeted NPs on the activation of microglia and macroglia, we did not observe a significant effect on the activation of PERK, one of the ER stress response pathways. Although in this study PERK does not appear to be a DHEA-modulated pathway, we cannot rule out the involvement of other ER stress pathways such as IRE1 and ATF6[65]. It is worth noting that DHEA can possibly also bind to “off-targets” other than S1R; therefore, we cannot exclude the possibility that the observed therapeutic effect of DHEA was partially mediated through other targets. Interestingly, it was recently reported that even DHEA activation of an “off-target”, the TrkA receptor, protected retinal neurons from excitotoxicity-induced cell loss[18]. Therefore, our results suggest that targeted NPs protect RGCs against NMDA-induced cytotoxicity likely through multiple molecular mechanisms. Nevertheless, the RGC-protecting effect of DHEA is potentiated by efficient local drug delivery achieved with the targeted unimolecular micelle nanoplatform.

5. CONCLUSIONS

In this study, we have achieved two main objectives. (1) We have engineered the first RGC-targeting intraocular delivery nanoplatform—*i.e.,* CTB-conjugated unimNP—that accumulate at the RGC layer and are likely taken up directly by these cells. (2) By applying this nanoplatform for DHEA delivery in an acute model of RGC death, we have commenced a translational campaign to test an RGC/S1R dual-targeted therapeutic paradigm. The two objectives are unified in the preclinical tests that indicate an efficacious and relatively

sustainable protection of RGCs by targeted NPs. To realize the full potential of this drug delivery system, it is warranted to test it in a chronic model of glaucoma in future investigations. In addition, in light of faster drug release from NPs at lower pHs, shorter entrapment of NPs inside the acidic endosome/lysosome compartments would prolong their therapeutic effects. To this end, the unimNPs are amenable to conjugation with an endosome-escaping peptide[66, 67]. In summary, further development and optimization of this unique CTB-conjugated unimNP intraocular drug delivery nanoplatform may ultimately lead to a viable treatment for glaucoma.

Supplementary Material

Refer to Web version on PubMed Central for supplementary material.

ACKNOWLEDGEMENTS

This work was supported by the National Eye Institute grant R01EY022678 and the Morgridge Institute for Research & the James Christenson Estate Macular Degeneration Research Award (to L.-W. Guo), the NIH grant 1K25CA166178 (to S. Gong), the NEI grant R01EY012223 (to R.W. Nickells), and the NEI grant P30EY016665 (to the University of Wisconsin Vision Core). We thank Dr. Beth Weaver and Jun Wan for assistance with fluorescence microscopy.

REFERENCES

[1]. Nickells RW, Howell GR, Soto I, John SW. Under pressure: cellular and molecular responses during glaucoma, a common neurodegeneration with axonopathy. Annual review of neuroscience. 2012; 35:153–179.

[2]. Martin PM, Ola MS, Agarwal N, Ganapathy V, Smith SB. The sigma receptor ligand (+)-pentazocine prevents apoptotic retinal ganglion cell death induced in vitro by homocysteine and glutamate, Brain research. Molecular brain research. 2004; 123:66–75. [PubMed: 15046867]

[3]. Dun Y, Thangaraju M, Prasad P, Ganapathy V, Smith SB. Prevention of excitotoxicity in primary retinal ganglion cells by (+)-pentazocine, a sigma receptor-1 specific ligand. Investigative ophthalmology & visual science. 2007; 48:4785–4794. [PubMed: 17898305]

[4]. Ha Y, Dun Y, Thangaraju M, Duplantier J, Dong Z, Liu K, Ganapathy V, Smith SB. Sigma receptor 1 modulates endoplasmic reticulum stress in retinal neurons. Investigative ophthalmology & visual science. 2011; 52:527–540. [PubMed: 20811050]

[5]. Tchedre KT, Huang RQ, Dibas A, Krishnamoorthy RR, Dillon GH, Yorio T. Sigma-1 receptor regulation of voltage-gated calcium channels involves a direct interaction. Investigative ophthalmology & visual science. 2008; 49:4993–5002. [PubMed: 18641291]

[6]. Mueller BH 2nd, Park Y, Ma HY, Dibas A, Ellis DZ, Clark AF, Yorio T. Sigma-1 receptor stimulation protects retinal ganglion cells from ischemia-like insult through the activation of extracellular-signal-regulated kinases 1/2. Experimental eye research. 2014; 128:156–169. [PubMed: 25305575]

[7]. Mavlyutov TA, Nickells RW, Guo LW. Accelerated retinal ganglion cell death in mice deficient in the Sigma-1 receptor. Molecular vision. 2011; 17:1034–1043. [PubMed: 21541278]

[8]. Smith SB, Duplantier J, Dun Y, Mysona B, Roon P, Martin PM, Ganapathy V. In vivo protection against retinal neurodegeneration by sigma receptor 1 ligand (+)-pentazocine. Invest Ophthalmol Vis Sci. 2008; 49:4154–4161. [PubMed: 18469181]

[9]. Ha Y, Saul A, Tawfik A, Zorrilla EP, Ganapathy V, Smith SB. Diabetes accelerates retinal ganglion cell dysfunction in mice lacking sigma receptor 1. Molecular vision. 2012; 18:2860–2870. [PubMed: 23233788]

[10]. Ha Y, Saul A, Tawfik A, Williams C, Bollinger K, Smith R, Tachikawa M, Zorrilla E, Ganapathy V, Smith SB. Late-onset inner retinal dysfunction in mice lacking sigma receptor 1 (sigmaR1). Investigative ophthalmology & visual science. 2011; 52:7749–7760. [PubMed: 21862648]

[11]. Hayashi T, Su TP. Sigma-1 receptor chaperones at the ER-mitochondrion interface regulate Ca(2+) signaling and cell survival. Cell. 2007; 131:596–610. [PubMed: 17981125]

[12]. Schmidt HR, Zheng S, Gurpinar E, Koehl A, Manglik A, Kruse AC. Crystal structure of the human sigma1 receptor. Nature. 2016; 532:527–530. [PubMed: 27042935]

[13]. Zhao J, Ha Y, Liou GI, Gonsalvez GB, Smith SB, Bollinger KE. Sigma receptor ligand, (+)-pentazocine, suppresses inflammatory responses of retinal microglia. Invest Ophthalmol Vis Sci. 2014; 55:3375–3384. [PubMed: 24812552]

[14]. Wang J, Saul A, Roon P, Smith SB. Activation of the molecular chaperone, sigma 1 receptor, preserves cone function in a murine model of inherited retinal degeneration. Proc Natl Acad Sci U S A. 2016; 113:E3764–3772. [PubMed: 27298364]

[15]. Wang J, Shanmugam A, Markand S, Zorrilla E, Ganapathy V, Smith SB. Sigma 1 receptor regulates the oxidative stress response in primary retinal Muller glial cells via NRF2 signaling and system xc(−), the Na(+)-independent glutamate-cystine exchanger. Free radical biology & medicine. 2015; 86:25–36. [PubMed: 25920363]

[16]. Su TP, London ED, Jaffe JH. Steroid binding at sigma receptors suggests a link between endocrine, nervous, and immune systems. Science. 1988; 240:219–221. [PubMed: 2832949]

[17]. Bucolo C, Drago F. Neuroactive steroids protect retinal tissue through sigma1 receptors. Basic & clinical pharmacology & toxicology. 2007; 100:214–216. [PubMed: 17309527]

[18]. Kokona D, Charalampopoulos I, Pediaditakis I, Gravanis A, Thermos K. The neurosteroid dehydroepiandrosterone (DHEA) protects the retina from AMPA-induced excitotoxicity: NGF TrkA receptor involvement. Neuropharmacology. 2012; 62:2106–2117. [PubMed: 22269901]

[19]. Bucolo C, Drago F. Effects of neurosteroids on ischemia-reperfusion injury in the rat retina: role of sigma1 recognition sites. European journal of pharmacology. 2004; 498:111–114. [PubMed: 15363983]

[20]. Thakur SS, Barnett NL, Donaldson MJ, Parekh HS. Intravitreal drug delivery in retinal disease: are we out of our depth? Expert opinion on drug delivery. 2014; 11:1575–1590. [PubMed: 24931577]

[21]. Kaur IP, Kakkar S. Nanotherapy for posterior eye diseases. Journal of controlled release : official journal of the Controlled Release Society. 2014; 193:100–112. [PubMed: 24862316]

[22]. Puntel A, Maeda A, Golczak M, Gao SQ, Yu G, Palczewski K, Lu ZR. Prolonged prevention of retinal degeneration with retinylamine loaded nanoparticles. Biomaterials. 2015; 44:103–110. [PubMed: 25617130]

[23]. Iwase T, Fu J, Yoshida T, Muramatsu D, Miki A, Hashida N, Lu L, Oveson B, Lima e Silva R, Seidel C, Yang M, Connelly S, Shen J, Han B, Wu M, Semenza GL, Hanes J, Campochiaro PA. Sustained delivery of a HIF-1 antagonist for ocular neovascularization. Journal of controlled release : official journal of the Controlled Release Society. 2013; 172:625–633. [PubMed: 24126220]

[24]. Kambhampati SP, Clunies-Ross AJ, Bhutto I, Mishra MK, Edwards M, McLeod DS, Kannan RM, Lutty G. Systemic and Intravitreal Delivery of Dendrimers to Activated Microglia/Macrophage in Ischemia/Reperfusion Mouse Retina. Investigative ophthalmology & visual science. 2015; 56:4413–4424. [PubMed: 26193917]

[25]. Lambert WS, Ruiz L, Crish SD, Wheeler LA, Calkins DJ. Brimonidine prevents axonal and somatic degeneration of retinal ganglion cell neurons. Molecular neurodegeneration. 2011; 6:4. [PubMed: 21232114]

[26]. Smith CA, Chauhan BC. Imaging retinal ganglion cells: enabling experimental technology for clinical application. Prog Retin Eye Res. 2015; 44:1–14. [PubMed: 25448921]

[27]. Nuschke AC, Farrell SR, Levesque JM, Chauhan BC. Assessment of retinal ganglion cell damage in glaucomatous optic neuropathy: Axon transport, injury and soma loss. Exp Eye Res. 2015; 141:111–124. [PubMed: 26070986]

[28]. Abbott CJ, Choe TE, Lusardi TA, Burgoyne CF, Wang L, Fortune B. Imaging axonal transport in the rat visual pathway. Biomedical optics express. 2013; 4:364–386. [PubMed: 23412846]

[29]. Prabaharan M, Grailer JJ, Pilla S, Steeber DA, Gong S. Folate-conjugated amphiphilic hyperbranched block copolymers based on Boltorn H40, poly(L-lactide) and poly(ethylene

glycol) for tumor-targeted drug delivery. Biomaterials. 2009; 30:3009–3019. [PubMed: 19250665]

[30]. Prabaharan M, Grailer JJ, Pilla S, Steeber DA, Gong SQ. Amphiphilic multi-arm-block copolymer conjugated with doxorubicin via pH-sensitive hydrazone bond for tumor-targeted drug delivery. Biomaterials. 2009; 30:5757–5766. [PubMed: 19643472]

[31]. Prabaharan M, Grailer JJ, Pilla S, Steeber DA, Gong SQ. Gold nanoparticles with a monolayer of doxorubicin-conjugated amphiphilic block copolymer for tumor-targeted drug delivery. Biomaterials. 2009; 30:6065–6075. [PubMed: 19674777]

[32]. Xiao Y, Hong H, Javadi A, Engle JW, Xu W, Yang Y, Zhang Y, Barnhart TE, Cai W, Gong S. Multifunctional unimolecular micelles for cancer-targeted drug delivery and positron emission tomography imaging. Biomaterials. 2012; 33:3071–3082. [PubMed: 22281424]

[33]. Guo J, Hong H, Chen G, Shi S, Zheng Q, Zhang Y, Theuer CP, Barnhart TE, Cai W, Gong S. Image-guided and tumor-targeted drug delivery with radiolabeled unimolecular micelles. Biomaterials. 2013; 34:8323–8332. [PubMed: 23932288]

[34]. Xu W, Siddiqui IA, Nihal M, Pilla S, Rosenthal K, Mukhtar H, Gong S. Aptamer-conjugated and doxorubicin-loaded unimolecular micelles for targeted therapy of prostate cancer. Biomaterials. 2013; 34:5244–5253. [PubMed: 23582862]

[35]. Xu W, Burke JF, Pilla S, Chen H, Jaskula-Sztul R, Gong S. Octreotide-functionalized and resveratrol-loaded unimolecular micelles for targeted neuroendocrine cancer therapy. Nanoscale. 2013; 5:9924–9933. [PubMed: 23986296]

[36]. Guo J, Hong H, Chen G, Shi S, Nayak TR, Theuer CP, Barnhart TE, Cai W, Gong S. Theranostic Unimolecular Micelles Based on Brush-Shaped Amphiphilic Block Copolymers for Tumor-Targeted Drug Delivery and Positron Emission Tomography Imaging. ACS applied materials & interfaces. 2014

[37]. Tagawa N, Tamanaka J, Fujinami A, Kobayashi Y, Takano T, Fukata S, Kuma K, Tada H, Amino N. Serum dehydroepiandrosterone, dehydroepiandrosterone sulfate, and pregnenolone sulfate concentrations in patients with hyperthyroidism and hypothyroidism. Clinical chemistry. 2000; 46:523–528. [PubMed: 10759476]

[38]. Brinkman AM, Chen G, Wang Y, Hedman CJ, Sherer NM, Havighurst TC, Gong S, Xu W. Aminoflavone-loaded EGFR-targeted unimolecular micelle nanoparticles exhibit anti-cancer effects in triple negative breast cancer. Biomaterials. 2016; 101:20–31. [PubMed: 27267625]

[39]. Li Y, Semaan SJ, Schlamp CL, Nickells RW. Dominant inheritance of retinal ganglion cell resistance to optic nerve crush in mice. BMC Neurosci. 2007; 8:19. [PubMed: 17338819]

[40]. Li Y, Schlamp CL, Nickells RW. Experimental induction of retinal ganglion cell death in adult mice. Invest Ophthalmol Vis Sci. 1999; 40:1004–1008. [PubMed: 10102300]

[41]. Mavlyutov TA, Epstein M, Guo LW. Subcellular localization of the sigma-1 receptor in retinal neurons - an electron microscopy study. Scientific reports. 2015; 5:10689. [PubMed: 26033680]

[42]. Schlamp CL, Montgomery AD, Nair C.E. Mac, Schuart C, Willmer DJ, Nickells RW. Evaluation of the percentage of ganglion cells in the ganglion cell layer of the rodent retina. Mol Vis. 2013; 19:1387–1396. [PubMed: 23825918]

[43]. Nair, C.E. Mac, Fernandes, KA., Schlamp, CL., Libby, RT., Nickells, RW. Tumor necrosis factor alpha has an early protective effect on retinal ganglion cells after optic nerve crush. Journal of neuroinflammation. 2014; 11:194. [PubMed: 25407441]

[44]. Nair, C.E. Mac, Schlamp, CL., Montgomery, AD., Shestopalov, VI., Nickells, RW. Retinal glial responses to optic nerve crush are attenuated in Bax-deficient mice and modulated by purinergic signaling pathways. Journal of neuroinflammation. 2016; 13:93. [PubMed: 27126275]

[45]. Shi X, Guo LW, Seedial SM, Si Y, Wang B, Takayama T, Suwanabol PA, Ghosh S, DiRenzo D, Liu B, Kent KC. TGF-beta/Smad3 inhibit vascular smooth muscle cell apoptosis through an autocrine signaling mechanism involving VEGF-A. Cell Death Dis. 2014; 5:e1317. [PubMed: 25010983]

[46]. Schlamp CL, Johnson EC, Li Y, Morrison JC, Nickells RW. Changes in Thy1 gene expression associated with damaged retinal ganglion cells. Mol Vis. 2001; 7:192–201. [PubMed: 11509915]

[47]. Nickells RW, Pelzel HR. Tools and resources for analyzing gene expression changes in glaucomatous neurodegeneration. Exp Eye Res. 2015; 141:99–110. [PubMed: 25999234]

[48]. Chen G, Wang L, Cordie T, Vokoun C, Eliceiri KW, Gong S. Multi-functional self-fluorescent unimolecular micelles for tumor-targeted drug delivery and bioimaging. Biomaterials. 2015; 47:41–50. [PubMed: 25682159]

[49]. Wilhelm S, Tavares AJ, Dai Q, Ohta S, Audet J, Dvorak HF, Chan WC. Analysis of nanoparticle delivery to tumours. Nature Reviews Materials. 2016; 1:16014.

[50]. Lu Y-J, Wei K-C, Ma C-CM, Yang S-Y, Chen J-P. Dual targeted delivery of doxorubicin to cancer cells using folate-conjugated magnetic multi-walled carbon nanotubes. Colloids and Surfaces B: Biointerfaces. 2012; 89:1–9. [PubMed: 21982868]

[51]. Dabin I, Barnstable CJ. Rat retinal Muller cells express Thy-1 following neuronal cell death. Glia. 1995; 14:23–32. [PubMed: 7615343]

[52]. Nair, C.E. Mac, Nickells, RW. Neuroinflammation in Glaucoma and Optic Nerve Damage. Progress in molecular biology and translational science. 2015; 134:343–363. [PubMed: 26310164]

[53]. Shanmugam A, Wang J, Markand S, Perry RL, Tawfik A, Zorrilla E, Ganapathy V, Smith SB. Sigma receptor 1 activation attenuates release of inflammatory cytokines MIP1gamma, MIP2, MIP3alpha, and IL12 (p40/p70) by retinal Muller glial cells. J Neurochem. 2015; 132:546–558. [PubMed: 25439327]

[54]. Kourrich S, Su TP, Fujimoto M, Bonci A. The sigma-1 receptor: roles in neuronal plasticity and disease. Trends in neurosciences. 2012; 35:762–771. [PubMed: 23102998]

[55]. Alqawlaq S, Sivak JM, Huzil JT, Ivanova MV, Flanagan JG, Beazely MA, Foldvari M. Preclinical development and ocular biodistribution of gemini-DNA nanoparticles after intravitreal and topical administration: towards non-invasive glaucoma gene therapy. Nanomedicine : nanotechnology, biology, and medicine. 2014; 10:1637–1647.

[56]. Zulliger R, Conley SM, Naash MI. Non-viral therapeutic approaches to ocular diseases: An overview and future directions. Journal of controlled release : official journal of the Controlled Release Society. 2015; 219:471–487. [PubMed: 26439665]

[57]. Khalin I, Alyautdin R, Kocherga G, Bakar MA. Targeted delivery of brain-derived neurotrophic factor for the treatment of blindness and deafness. International journal of nanomedicine. 2015; 10:3245–3267. [PubMed: 25995632]

[58]. Pita-Thomas DW, Goldberg JL. Nanotechnology and glaucoma: little particles for a big disease. Current opinion in ophthalmology. 2013; 24:130–135. [PubMed: 23287105]

[59]. Kim KE, Jang I, Moon H, Kim YJ, Jeoung JW, Park KH, Kim H. Neuroprotective Effects of Human Serum Albumin Nanoparticles Loaded With Brimonidine on Retinal Ganglion Cells in Optic Nerve Crush Model. Invest Ophthalmol Vis Sci. 2015; 56:5641–5649. [PubMed: 26313300]

[60]. Mesentier-Louro LA, Zaverucha-do-Valle C, da Silva-Junior AJ, Nascimento-Dos-Santos G, Gubert F, de Figueiredo AB, Torres AL, Paredes BD, Teixeira C, Tovar-Moll F, Mendez-Otero R, Santiago MF. Distribution of mesenchymal stem cells and effects on neuronal survival and axon regeneration after optic nerve crush and cell therapy. PLoS ONE. 2014; 9:e110722. [PubMed: 25347773]

[61]. Hedskog L, Pinho CM, Filadi R, Ronnback A, Hertwig L, Wiehager B, Larssen P, Gellhaar S, Sandebring A, Westerlund M, Graff C, Winblad B, Galter D, Behbahani H, Pizzo P, Glaser E, Ankarcrona M. Modulation of the endoplasmic reticulum-mitochondria interface in Alzheimer's disease and related models. Proc Natl Acad Sci U S A. 2013; 110:7916–7921. [PubMed: 23620518]

[62]. Francardo V, Bez F, Wieloch T, Nissbrandt H, Ruscher K, Cenci MA. Pharmacological stimulation of sigma-1 receptors has neurorestorative effects in experimental parkinsonism. Brain : a journal of neurology. 2014; 137:1998–2014. [PubMed: 24755275]

[63]. Mavlyutov TA, Epstein ML, Verbny YI, Huerta MS, Zaitoun I, Ziskind-Conhaim L, Ruoho AE. Lack of sigma-1 receptor exacerbates ALS progression in mice. Neuroscience. 2013; 240:129–134. [PubMed: 23458708]

[64]. Mavlyutov TA, Guo LW, Epstein ML, Ruoho AE. Role of the Sigma-1 receptor in Amyotrophic Lateral Sclerosis (ALS). Journal of pharmacological sciences. 2015; 127:10–16. [PubMed: 25704013]

[65]. Mori T, Hayashi T, Hayashi E, Su TP. Sigma-1 receptor chaperone at the ER-mitochondrion interface mediates the mitochondrion-ER-nucleus signaling for cellular survival. PloS one. 2013; 8:e76941. [PubMed: 24204710]

[66]. Erazo-Oliveras A, Muthukrishnan N, Baker R, Wang TY, Pellois JP. Improving the endosomal escape of cell-penetrating peptides and their cargos: strategies and challenges. Pharmaceuticals (Basel). 2012; 5:1177–1209. [PubMed: 24223492]

[67]. Nouri FS, Wang X, Dorrani M, Karjoo Z, Hatefi A. A recombinant biopolymeric platform for reliable evaluation of the activity of pH-responsive amphiphile fusogenic peptides. Biomacromolecules. 2013; 14:2033–2040. [PubMed: 23682625]

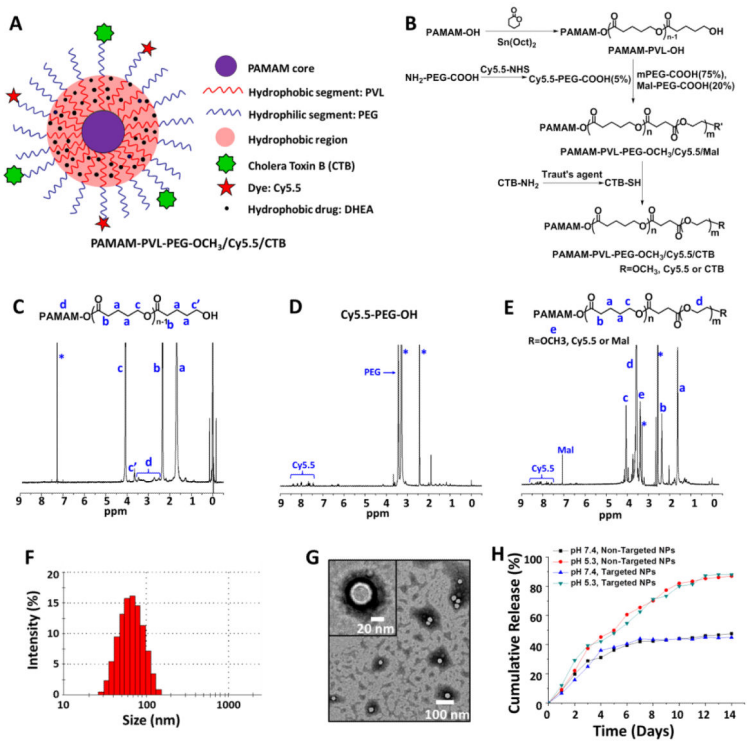

Figure 1. Synthesis and characterization of targeted and non-targeted unimNPs

(A) A schematic illustration of multifunctional unimolecular micelle nanoparticles formed by multi-arm star amphiphilic block copolymer PAMAM–PVL–PEG–Cy5.5/CTB for targeted delivery of DHEA to RGCs. **(B)** Synthesis scheme of multi-arm star amphiphilic block copolymer PAMAM–PVL–PEG–Cy5.5/CTB. ^{1}H NMR spectra of **(C)** PAMAM–PVL–OH, **(D)** Cy5.5–PEG–COOH, and **(E)** PAMAM–PVL–PEG–OCH_3/Cy5.5/Mal. **(F)** DLS analysis and **(G)** TEM images of the unimNPs. **(H)** *In vitro* DHEA release profiles from DHEA-loaded, non-targeted and targeted unimNPs at two different pHs.

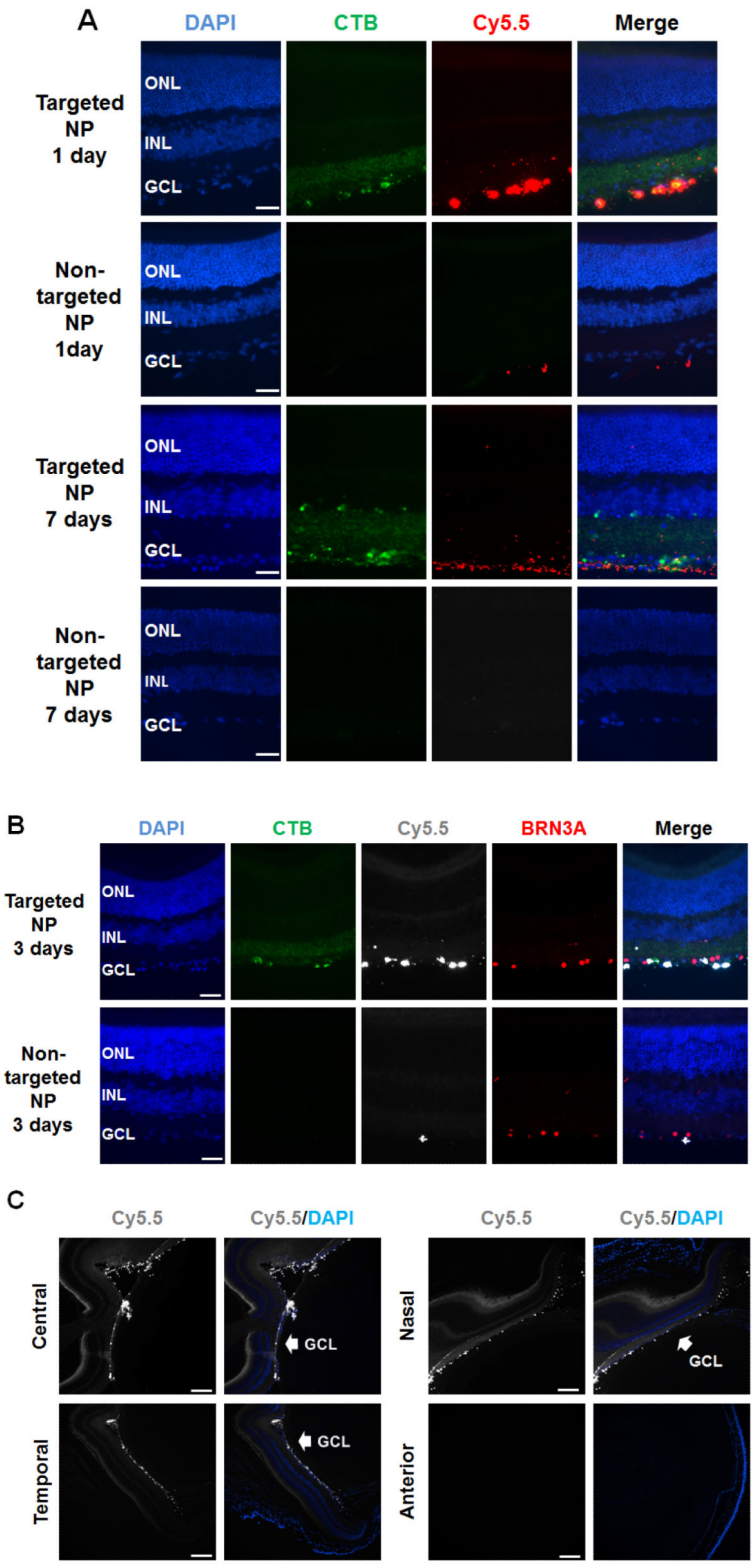

Figure 2. Accumulation of targeted NPs at the mouse RGC layer after intravitreal injection

Targeted NPs (i.e., DHEA-loaded CTB-unimNPs) and non-targeted NPs control (i.e., DHEA-loaded unimNPs), both mixed with NMDA, were injected respectively into the right eye (or left eye, randomly assigned) of two separate groups of mice,. Each injection (total 2 μl) contained 0.5 μg DHEA, 40 mM NMDA, and 2 μg unimNP. At 1, 3, and 7 days after injection, mice were euthanized and retinal sections prepared for fluorescence microscopy. Retinal layers were distinguished by DAPI staining: ONL, outer nuclear layer; INL, inner nuclear layer; GCL, retinal ganglion cell (RGC) layer. (**A**) Localization of NP (Cy5.5-conjugated, red). While targeted NPs were accumulated at the RGC layer, non-targeted NPs were barely detectable. CTB was labeled green (FITC). (**B**) Co-localization of NP (white, pseudo-color) with RGCs, which were detected by immunostaining of the marker protein BRN3A (red). (**C**) Overview of the entire mouse eye section showing accumulation of targeted NPs (white, pseudo-color) along GCL in the retina. The anterior image shows the cornea which is Cy5.5 negative. Scale bar: A and B, 50 μm; C, 200 μm.

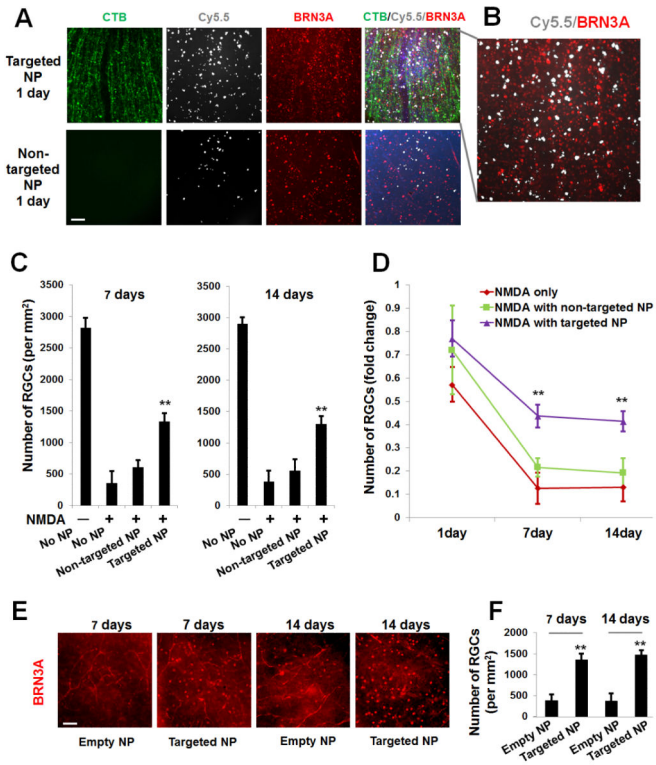

Figure 3. Rescue of RGCs by targeted NPs following intravitreal injection (counting on whole-mounts)

Intravitreal injections were performed as described in Figure 2. Mice were euthanized at indicated time points and retinal whole mounts were prepared for fluorescence microscopy. (**A**) Representative images showing distribution of CTB (green), Cy5.5 (white), and BRN3A-positive nuclei (red). Scale bar: 100 μm. (**B**). Enlarged image in A showing Cy5.5 and BRN3A. (**C**). Quantification of BRN3A-positive cells: mean ± SE; n = 7–10 animals. **P < 0.01, compared to NMDA only (no NPs). (**D**). Data are re-plotted as time course of nuclei number fold change versus vehicle (DMSO) control. **P < 0.01 compared to NMDA only (no NPs). The data show that while targeted NPs preserved RGC layer cells, non-targeted NPs had no significant effect. (**E**) Representative images showing BRN3A-positive nuclei of retinal whole mounts collected at 7 and 14 days after injection of CTB-unimNPs without (empty NP) or with (targeted NP) DHEA loaded (the same amount as in A). Scale bar: 100 μm. (**F**). Quantification of BRN3A-positive cells in E: mean ± SE; n = 7–10 animals. **P < 0.01, compared to empty NPs.

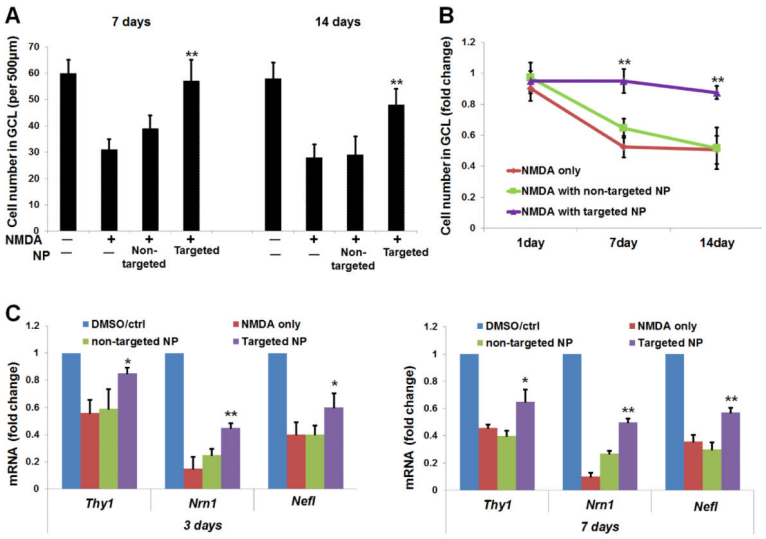

Figure 4. Rescue of RGCs by targeted NPs following intravitreal injection (counting on vertical sections)

Injections were performed as described in Figure 2. Eyeballs were collected at indicated time points after injection for the preparation of retinal sections (nuclei counting) or homogenates (RT-PCR). Quantification: mean ± SE; n = 7–10 animals. (**A**) The number of nuclei (per 500 μm retina length) was counted at the RGC layer. **P < 0.01, compared to NMDA only (no NPs). (**B**) Data are re-plotted as time course of nuclei number fold change versus vehicle (DMSO) control. **P < 0.01 compared to NMDA only (no NPs). The data show that while targeted NPs preserved RGC layer cells, non-targeted NPs had no significant effect. (**C**) Expression of RGC marker genes was determined by qRT-PCR. **P < 0.01, *P < 0.05, compared to NMDA only.

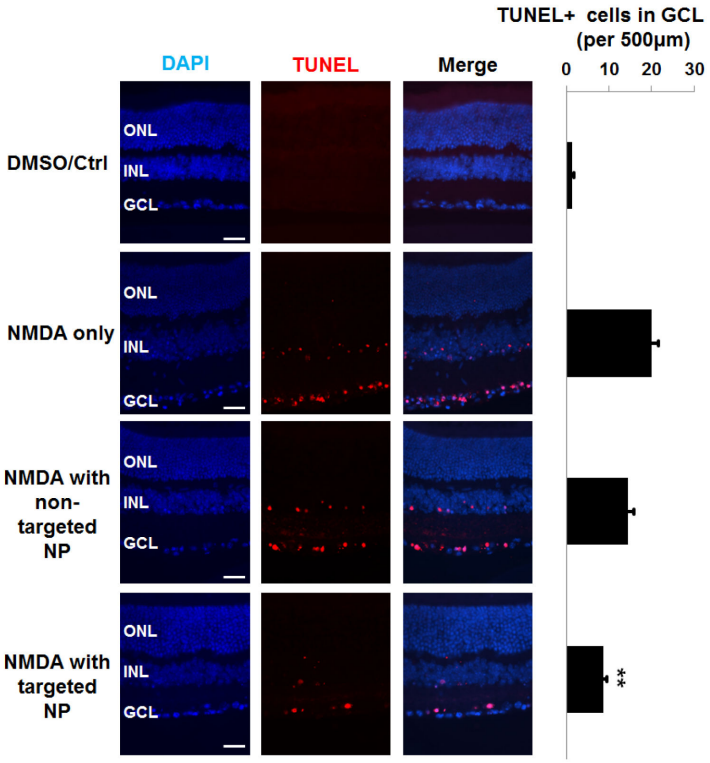

Figure 5. Prevention of NMDA-induced increase of TUNEL-positive cells by targeted NPs following intravitreal injection

Injections were performed as described in Figure 2. Eyeballs were collected at 1 day after injection. TUNEL staining was performed on retinal cryosections. Scale Bar: 50 μm. Quantification: mean ± SE of TUNEL-positive nuclei at the RGC layer (per 500 μm retina length); n > 5 animals; **P < 0.01 compared to NMDA alone.

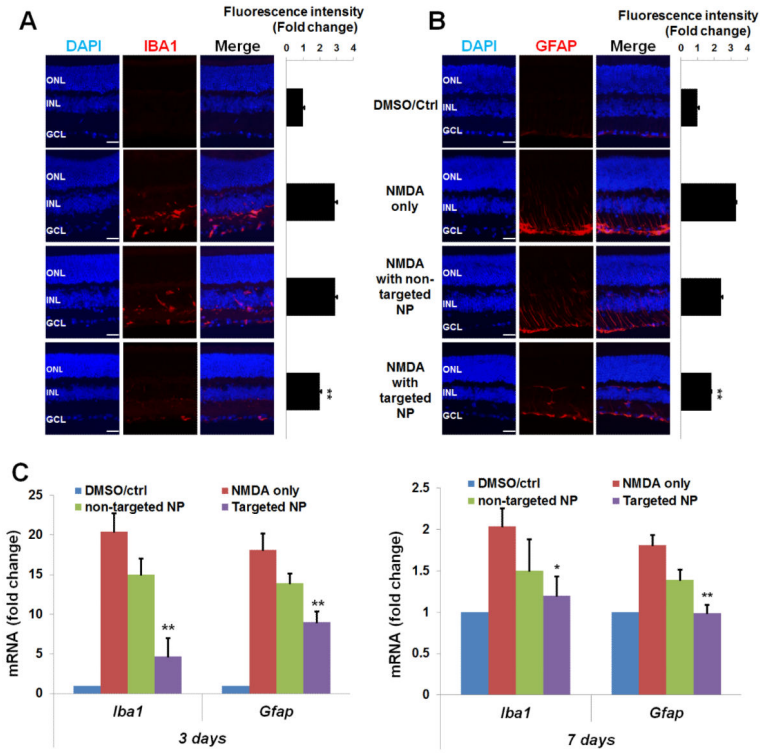

Figure 6. Inhibition of NMDA-induced activation of retinal microglia and macroglia by targeted NPs following intravitreal injection

Injections were performed as described in Figure 2. Eyeballs were collected for preparation of retinal cryosections (immunohistochemistry) or homogenates (qRT-PCR). Quantification: mean ± SE; normalization to vehicle control; n > 5 animals; **P < 0.01, *P < 0.05, compared to NMDA only. Immunostaining of (**A**) IBA1 or (**B**) GFAP were performed on retinal sections collected 3 days after injection and the area including INL and GCL was used for quantification. Scale bar: 50 μm. (**C**) Levels of mRNA of *Iba1* and *Gfap* were determined by qRT-PCR using unfixed samples collected at 3 or 7 days after injection.

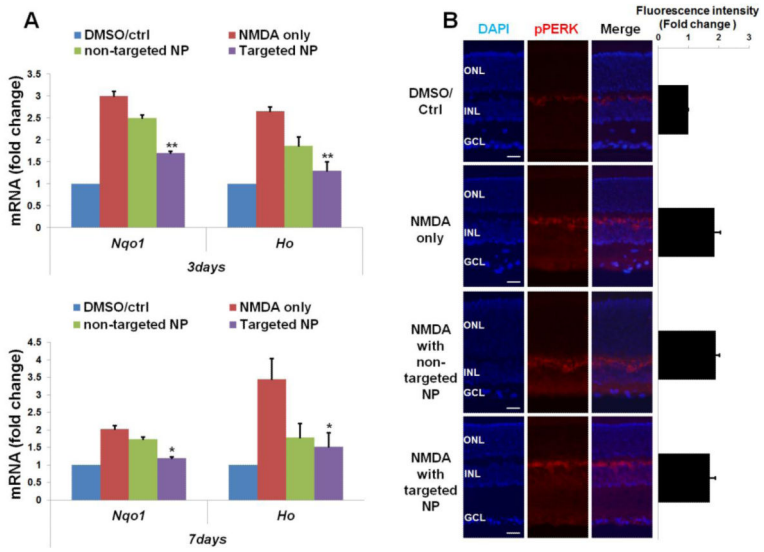

Figure 7. Reduction of NMDA-induced oxidative stress by targeted NPs following intravitreal injection

Injections were performed as described in Figure 2. Eyeballs were collected for preparation of retinal cryosections (immunohistochemistry) or homogenates (RT-PCR). Quantification: mean ± SE; normalization to vehicle control; n > 5 animals; **P < 0.01, *P < 0.05, compared to NMDA only. (**A**) Levels of mRNA of *Nqo1* and *Ho1* were determined by RT-PCR using unfixed samples collected at 3 or 7 days after injection. (**B**) Immuno-staining of pPERK performed on retinal sections collected at 3 days after injection and the area including INL and GCL was used for quantification. Scale bar: 50 μm.

Author Manuscript

Author Manuscript

Author Manuscript

Table 1

Molecular weights of all polymers.

Polymers	M_n (g/mol)	M_w(g/mol)	PDI (M_w/M_n)
PAMAM–OH	14277	—	—
PAMAM–PVL–OH	99450	141616	1.424
PAMAM–PVL–PEG–OCH_3/Cy5.5/Mal	252317	376660	1.48